Appendices

- **Electronic Supplement A: Additional data and results**
- **Electronic Supplement B: Additional considerations**

A Electronic Supplement A: Additional data and results

The following figures provide additional data and results, and are referenced throughout the article.

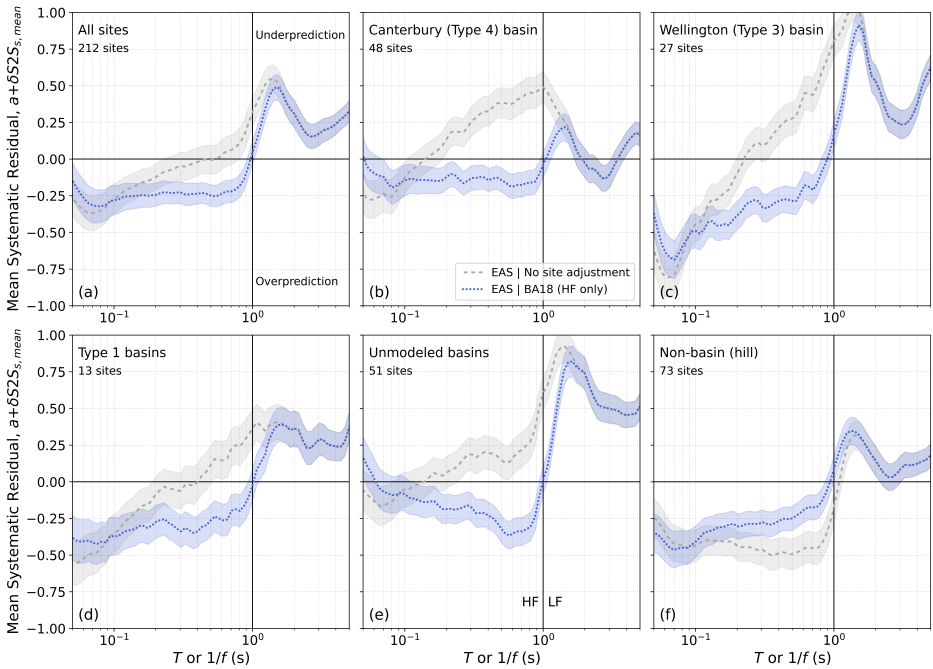

Figure A.1. Mean systematic residual, $a + \delta S2S_{s,mean}$, for EAS, for the simulation with no site adjustment and for the (HF only) BA18 model. The mean systematic residuals are plotted for (a) all sites, and for (b) Canterbury (Type 4) basin, (c) Wellington (Type 3), (d) Type 1 basin, (e) unmodeled basin, and (f) non-basin (hill) sites. The shaded areas in the plot represent the 95% confidence interval for the mean systematic residual, which accounts for uncertainty in both the fixed effect a and the mean of the random effects $\delta S2S_s$ per category.

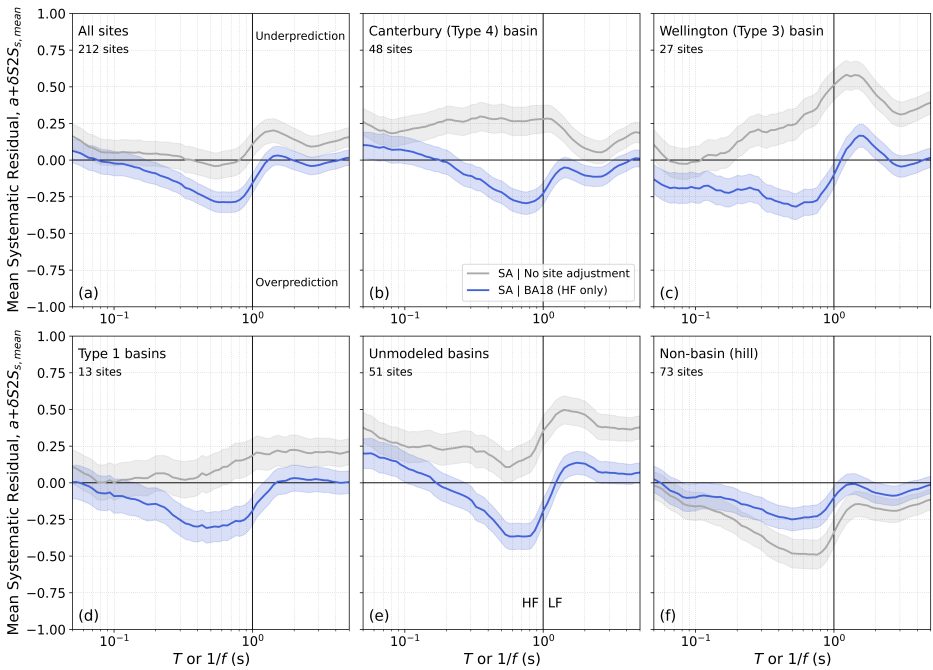

Figure A.2. Mean systematic residual, $a + \delta S2S_{s,mean}$, for SA, for the simulation with no site adjustment and for the (HF only) BA18 model. The mean systematic residuals are plotted for (a) all sites, and for (b) Canterbury (Type 4) basin, (c) Wellington (Type 3), (d) Type 1 basin, (e) unmodeled basin, and (f) non-basin (hill) sites. The shaded areas in the plot represent the 95% confidence interval for the mean systematic residual, which accounts for uncertainty in both the fixed effect a and the mean of the random effects $\delta S2S_s$ per category.

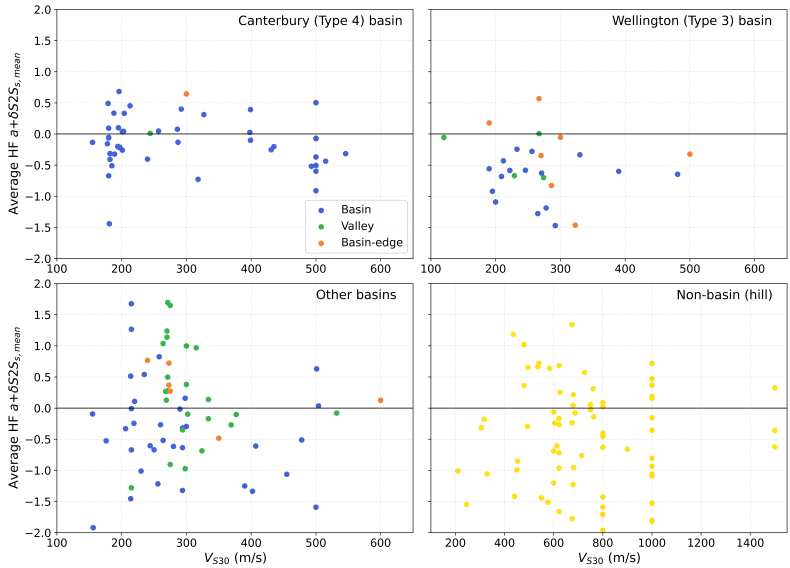

Figure A.3. Dependency between the EAS systematic site residual averaged over the $f = 10 - 20$ Hz range, and V_{S30}.

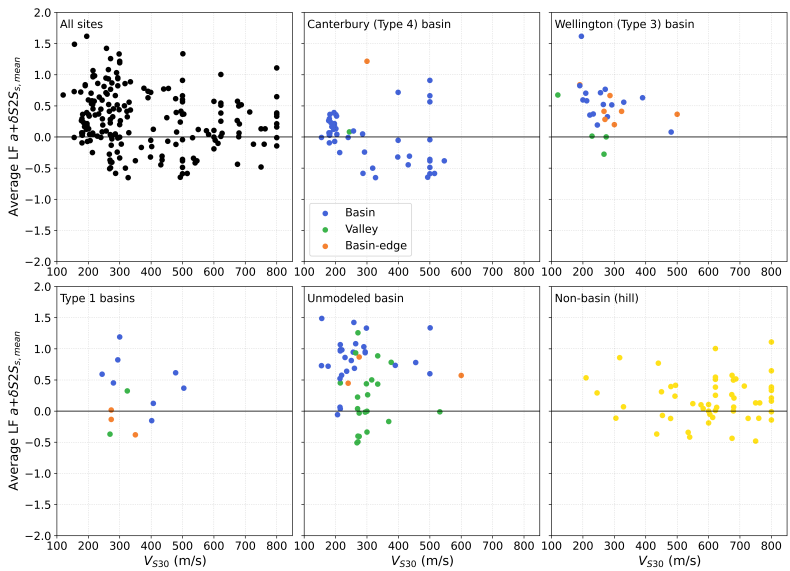

Figure A.4. Dependency between the EAS systematic site residual averaged over the $f = 0.3 - 1.0$ Hz range, and V_{S30}.

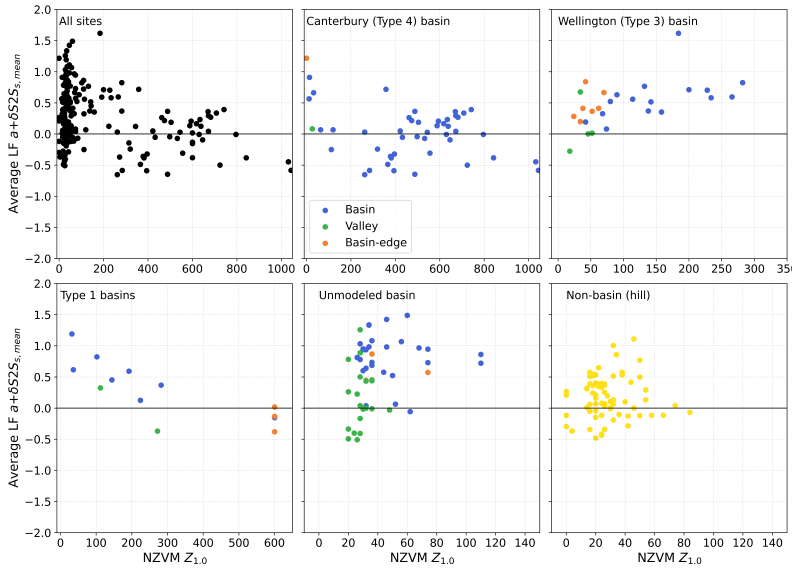

Figure A.5. Dependency between the EAS systematic site residual averaged over the $f = 0.3 - 1.0$ Hz range, and $Z_{1.0}$.

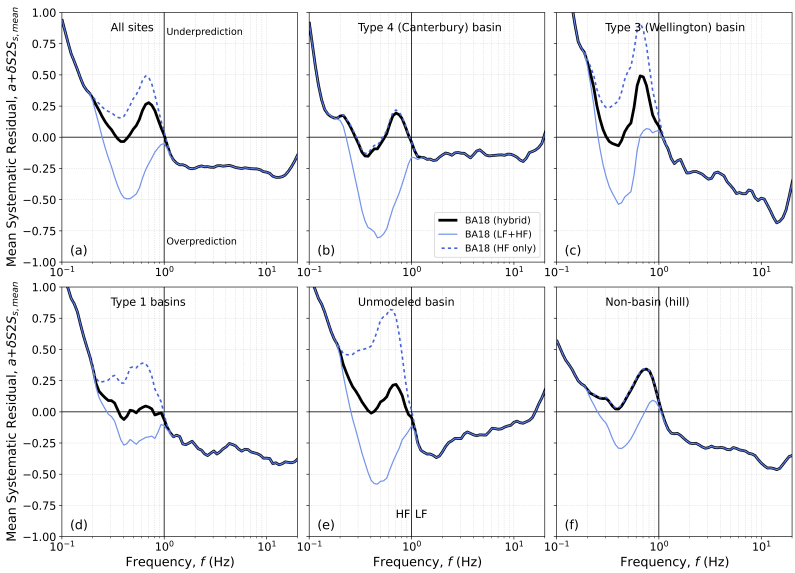

Figure A.6. Mean EAS systematic residual, $a + \delta S2S_{s,mean}$, for the BA18 model, using alternative SF application protocols. The mean systematic residuals are plotted for (a) all sites, and for (b) Canterbury (Type 4) basin, (c) Wellington (Type 3), (d) Type 1 basin, (e) unmodeled basin, and (f) non-basin (hill) sites.

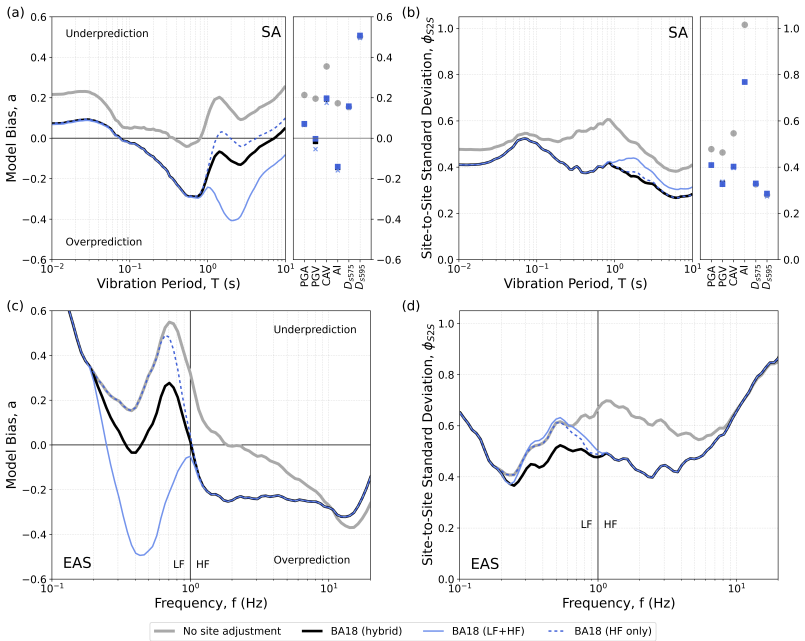

Figure A.7. Model prediction bias, a, and site-to-site standard deviation, ϕ_{S2S}, for the BA18 model, using alternative SF application protocols. (a) a and (b) ϕ_{S2S} for SA, PGA, PGV, CAV, AI, D_{s575}, and D_{s595}. (c) a and (d) ϕ_{S2S} for EAS.

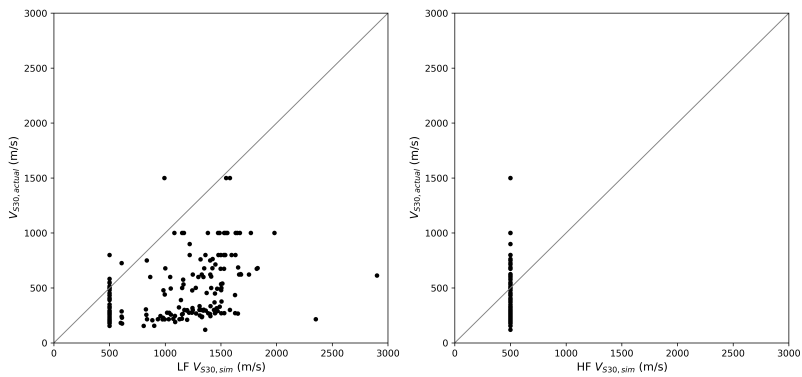

Figure A.8. Comparison between $V_{S30,actual}$ values and the corresponding (a) LF and (b) HF $V_{S30,sim}$ values.

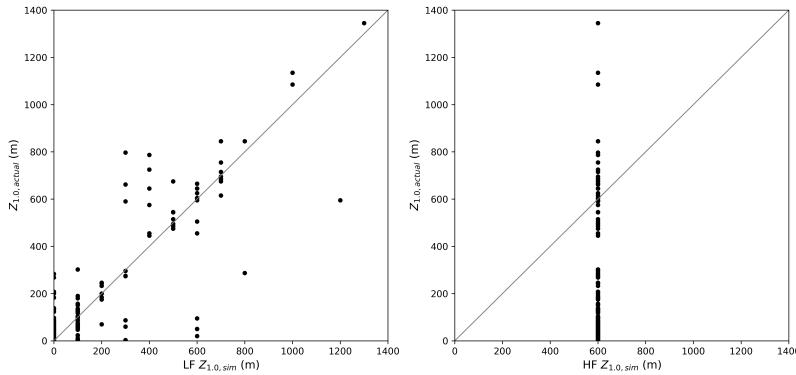

Figure A.9. Comparison between $Z_{1.0,actual}$ values and the corresponding (a) LF and (b) HF $Z_{1.0,sim}$ values.

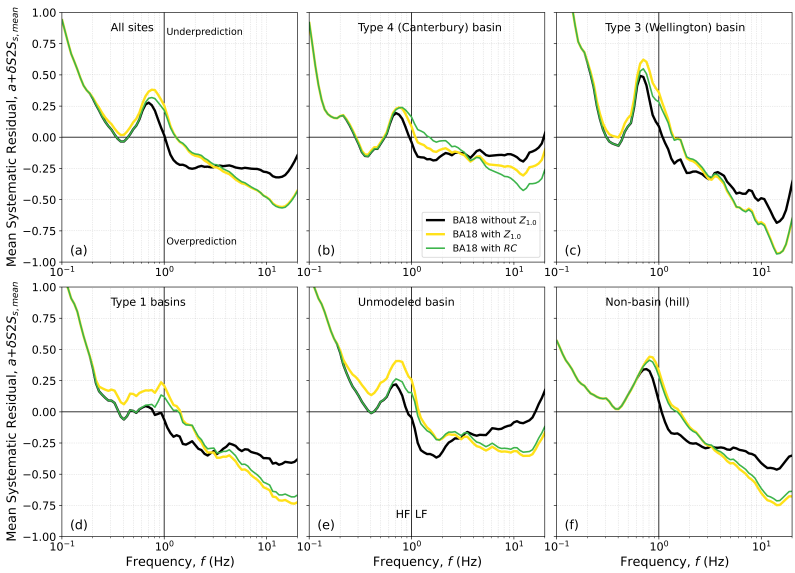

Figure A.10. Mean EAS systematic residual, $a + \delta S2S_{s,mean}$, for the BA18 model, considering the 'hybrid" SF application protocol, and including different adjustments. The mean systematic residuals are plotted for (a) all sites, and for (b) Canterbury (Type 4) basin, (c) Wellington (Type 3), (d) Type 1 basin, (e) unmodeled basin, and (f) non-basin (hill) sites.

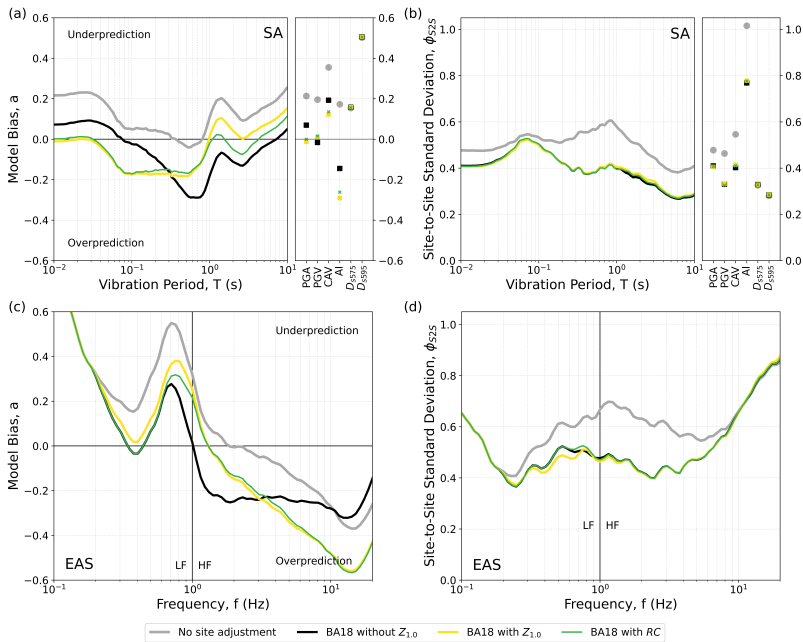

Figure A.11. Model prediction bias, a, and site-to-site standard deviation, ϕ_{S2S}, for the BA18 model, considering the "hybrid" SF application protocol, and including different adjustments. (a) a and (b) ϕ_{S2S} for SA, PGA, PGV, CAV, AI, D_{s575}, and D_{s595}. (c) a and (d) ϕ_{S2S} for EAS.

B Electronic Supplement B: Additional considerations

Figure B.1 presents the linear site amplification factor (relative to $V_{S30} = 760$ m/s) predicted by the BA18, CB24, CB14, and BSSA14 models as a function of V_{S30}, at 0.5 and 10 Hz. At large V_{S30}, the BA18 and BSSA14 models limit the site amplification to a constant value, whereas the CB24 and CB14 models continue to reduce the site amplification as V_{S30} increases. As noticed by Bradley (2013), this continued reduction may be justified at high frequencies but not at low frequencies. This is due to the correlation between V_{S30} and V_S at depth (e.g., Kamai et al. 2016), which suggests that at very stiff rock sites, changes in V_{S30} mainly reflect variations in the shallow part of the velocity profile, affecting primarily the high-frequency ground motion. Figure B.1a shows that the CB24 and CB14 models predict changes in amplification even at 0.5 Hz, which is inconsistent with this expectation.

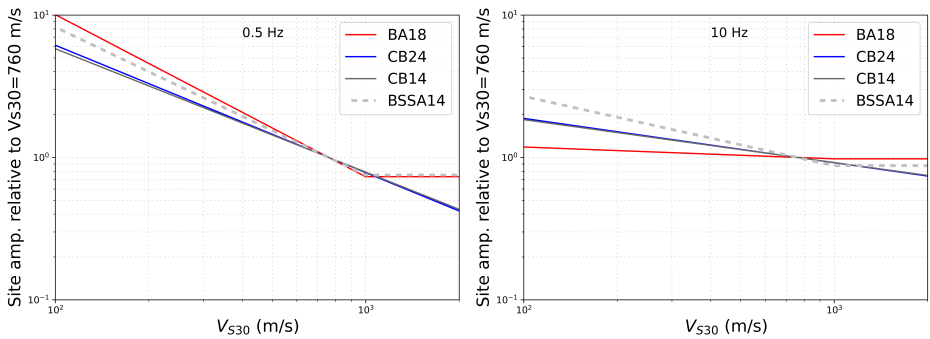

Figure B.1. Linear site amplification factors (relative to $V_{S30} = 760$ m/s versus V_{30} for the BA18, CB24, CB14, and BSSA14 models, at (a) 0.5 Hz and (b) 10 Hz.

As shown in Figure A.9, most $V_{S30,actual}$ values in this study are below 1000 m/s. However, a considerable portion of the $V_{S30,sim}$ values are significantly larger. For example, 17% exceed 1500 m/s. This implies that, at several sites, the low-frequency site amplification may be unrealistically large when using the CB24 and CB14 models.